Supporting Information

Functionalisation of MoS_2 2D layers with diarylethene molecules

†Marc Morant-Giner,[a] †José M. Carbonell-Vilar,[a] Marta Viciano-Chumillas,[a,*] Alicia Forment-Aliaga,[a,*] Joan Cano,[a] Eugenio Coronado[a]

1 Experimental

Materials

All chemicals were obtained from commercial sources and used as received. 1,2-bis(5-chloro-2-methylthien-3-yl)cyclopentene (**a**) and 1,2-bis(2-methyl-5-phenylthien-3-yl)cyclopentene (**3-H**) were synthesised following the reported procedures.[1] ce-MoS_2 was synthesised by solvothermal lithium intercalation according to the reported procedure.[2]

Caution! Diazonium salts are potentially explosive. They should be used in small quantities and be treated with the utmost care at all times.

1.1 Syntheses of the organic molecules

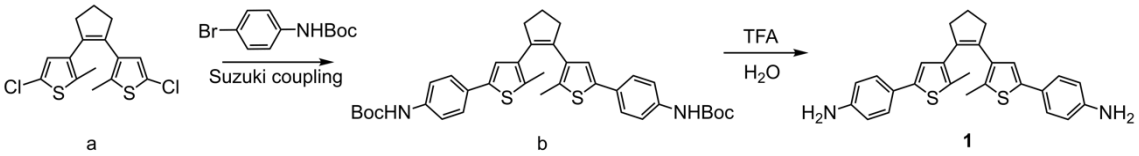

Scheme 1. Synthetic procedure of **1**.

1,2-Bis[2-methyl-5-(4-*N*-(*tert*-butoxycarbonyl)-aminophenyl)-3-thienyl]cyclopentene (b). a (0.58 g, 1.76 mmol) and 13 mL of dry THF were added into a two-necked flask under an argon atmosphere. Then, *n*-butyllithium (2.30 mL, 3.69 mmol, 1.6 M in hexane) was very slowly added, giving a black solution. Next, tributyl borate (1.42 mL, 5.26 mmol) was quickly added affording an orange solution, which was stirred for 1 h at room temperature. Then, *N*-(*tert*-butoxycarbonyl)-4-bromoaniline (1.43 mg, 5.27 mmol), $Pd(PPh_3)_4$ (203 mg, 0.18 mmol), sodium carbonate (11.40 mL, 22.83 mmol, 2 M in H_2O) and few drops of ethylene glycol were added sequentially to the reaction mixture, which was refluxed overnight. The reaction cooled down to room temperature and, then, H_2O (120 mL) was added. Liquid-liquid extraction was performed by adding ethyl acetate (2 × 55 mL). The organic phase was washed with brine, dried over magnesium sulphate, and the solvent was removed in a rotary evaporator giving a reddish-brown oil. The product was purified by column chromatography on silica gel (8.5 hexane: 1.5 ethyl acetate) affording a brown solid (0.64 g, 60%). ^{1}H-NMR (300 MHz, $CDCl_3$) δ = 7.43 (d, *J* = 8.62 Hz, 4H, phenyl), 7.34 (d, *J* = 8.80 Hz, 4H, phenyl), 6.97 (s, 2H, thiophene), 6.60 (s, 2H, NH), 2.85 (t, *J* = 7.52 Hz, 4H, cyclopentene), 2.08 (qt, *J* = 7.52 Hz, 2H, cyclopentene), 1.99 (s, 6H, CH_3), 1.54 (s, 18H, CH_3).

1,2-Bis[2-methyl-5-(4-aminophenyl)-3-thienyl]cyclopentene (1o). b (0.64 g, 1 mmol) was dissolved in dichloromethane (25 mL). Next, trifluoroacetic acid (2.48 mL, 53.08 mmol) was added and stirred vigorously overnight and, later, the solvent was removed in a rotary evaporator. Saturated sodium bicarbonate (35 mL) was added and extracted with dichloromethane (6 × 20 mL). The organic phase was collected, dried over magnesium sulphate and filtered under vacuum, giving a red solution. The solvent was removed in a rotary evaporator to yield a grey solid, which was filtered off and washed with diethyl ether. Again, the red solution was evaporated with a rotary evaporator giving a brown powder used without further purification (0.38 g, 85%). ^{1}H-NMR (300 MHz, $CDCl_3$) δ = 7.31 (d, *J* = 8.62 Hz, 4H, phenyl), 6.88 (s, 2H, thiophene), 6.66 (d, *J* = 8.62 Hz, 4H, phenyl), 2.83 (t, *J* = 7.43 Hz, 4H, cyclopentene), 2.06 (qt, *J* = 7.38 Hz, 2H, cyclopentene), 1.97 (s, 6H, CH_3). HRMS *m/z* 443.1590 ($[M + H]^+$, calculated for $C_{27}H_{27}N_2S_2$, 443.1616).

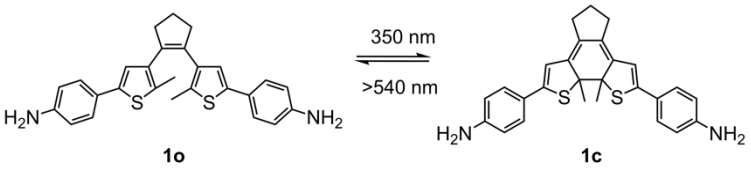

Scheme 2. Photoswitching behaviour of **1**.

Closed-ring isomer of 1o (1c). 1o (0.7 mM) in MeOH was placed in a beaker with stirring and then subjected to UV irradiation (350 nm) in a photoreactor for approximately 15 min. A dark purple solution was obtained, which was rotary evaporated to afford a dark purple solid, and it was used without any purification and isolation.

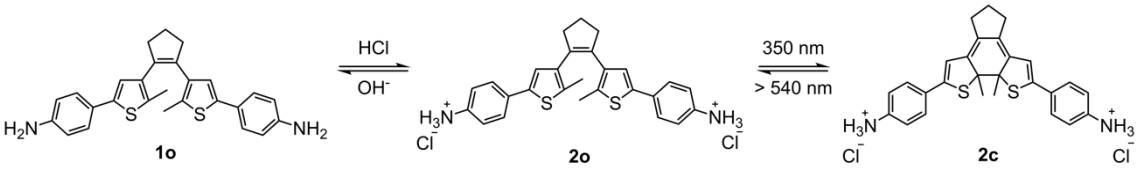

Scheme 3. Synthetic route and photoswitching behaviour of **2**.

1,2-Bis[2-methyl-5-(4-aminophenyl)-3-thienyl]cyclopentene hydrochloride (2o). To a EtOH/H_2O solution (2:1, 68 mL) of **1o** (12.30 mg, 0.028 mmol), HCl 6 M (18 µL, 0.108 mmol) was added. Then, the obtained grey-yellow solution was precipitated with diethyl ether, affording a grey solid, which was used without purification. IR (ν_{max}/cm^{-1}): 3442(vs, br), 2911(s), 2839(s), 2583(m), 1616(m), 1540(m), 1509(s), 1473(vw), 1437(w), 1311(vw), 1288(vw), 1210(w), 1117(w), 1016(vw), 948(vw), 820(m), 755(vw), 678(vw), 659(vw), 634(w), 558(vw), 487(m), 473(w), 429(w).

Closed-ring isomer of 2o (2c). 1o (12.30 mg, 0.028 mmol) was dissolved in EtOH/H_2O (2:1, 68 mL) and HCl 6M (18 µL, 0.108 mmol) was added. Then, the solution was placed in a beaker with stirring and then subjected to UV irradiation (350 nm) in a photoreactor for approximately 10 min. A dark violet solution was obtained and it was used without any purification nor isolation. IR (ν_{max}/cm^{-1}): 3399(m, br), 3178(m), 2920(vs), 2851(vs), 2567(s), 1604(s), 1560(m), 1509(s), 1471(s), 1425(s), 1349(m), 1315(s), 1269(s), 1177(vs), 1163(vs), 1076(m), 1059(m), 1019(w), 997(s), 921(w), 894(m), 821(m), 743(vw), 669(vw), 632(vw), 542(w), 487(w).

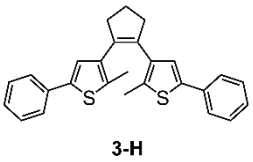

Scheme 4. Molecular structure of **3-H**.

Closed ring isomer of 3-Ho (3-Hc). 3-Ho (0.20 g, 0.485 mmol) was dissolved in hexane (100 mL) and then subjected to UV irradiation (308 nm) in a photoreactor for 1 h and 15 minutes giving a dark purple solution. The compound was crystallised by slow evaporation in acetonitrile yielding a mixture of dark purple and colourless crystals as minor impurities, which were removed manually. ^{1}H-NMR (300 MHz, $CDCl_3$) δ = 7.52 (t, *J* = 7.76 Hz, 4H, phenyl), 7.36 (t, *J* = 7.06 Hz, 4H, phenyl), 7.32 (t, *J* = 6.60 Hz, 2H, phenyl), 6.42 (s, 2H, thiophene), 2.50 (t, *J* = 7.34 Hz, 4H, cyclopentene), 2.03 (s, 6H, CH_3), 1.92 (qt, *J* = 7.29 Hz, 2H, cyclopentene).

1.2 Molecular functionalisation

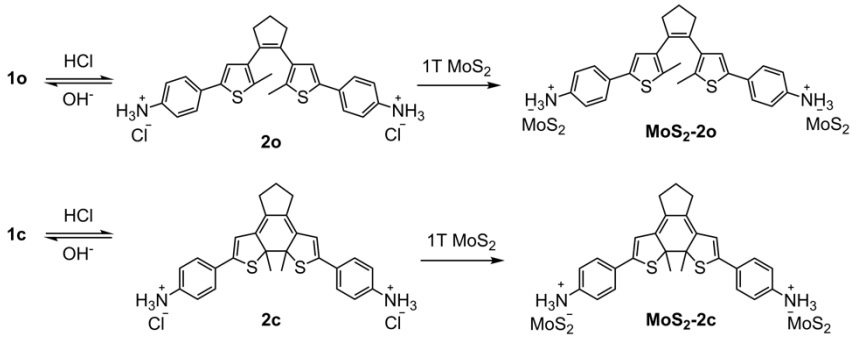

Scheme 5. Electrostatic functionalisation of **MoS_2-2**.

MoS_2-2o. To a solution of **1o** (43.97 mg, 0.1 mmol) in EtOH/H_2O (2:1, 180 mL), HCl 6M (64.4 µL) was added to afford **2o** with the resulting colour change from salmon to grey-yellow ($pH_{theo} \approx 2.8$). Then, an aqueous solution of ce-MoS_2 (0.1 mmol) was added dropwise under an inert atmosphere. The reaction mixture was stirred for 30 minutes yielding a black suspension. The suspension was centrifuged, and a black solid was collected. Then, it was washed with a mixture of EtOH/H_2O (2:1), and then dried under vacuum in the darkness.

MoS_2-2c. **1o** (43.97 mg, 0.1 mmol) was dissolved in EtOH/H_2O (1:1, 244 mL) and then, HCl 6M (64.4 µL) was added. Next, the reaction mixture was subjected to UV irradiation (350 nm) in a photoreactor for 10 min to afford **2c**. An aqueous solution of ce-MoS_2 (0.1 mmol) was added dropwise under an inert atmosphere. The reaction mixture was stirred for 30 minutes yielding a black suspension. The suspension was centrifuged. The remaining solid was washed with a mixture of EtOH/H_2O (2:1), then dried under vacuum.

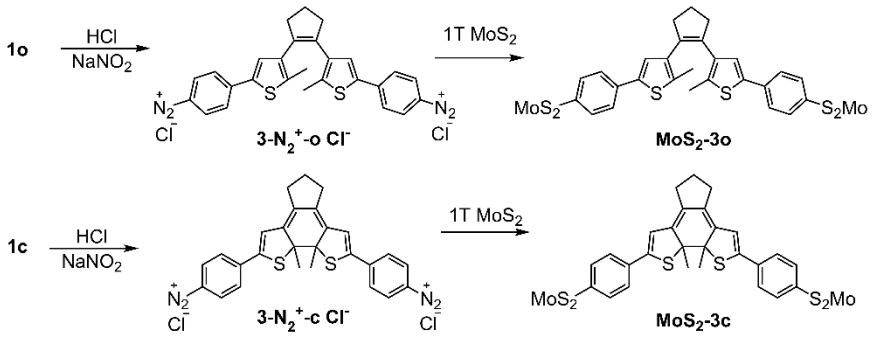

Scheme 6. Covalent functionalisation of **MoS_2-3**.

MoS_2-3o. 1o (12.30 mg, 0.028 mmol) was suspended in water under an argon atmosphere. Subsequently, sodium nitrite (5.77 mg, 0.084 mmol) and HCl 6 M (511 µL) were added at 0 °C, and the resultant mixture was stirred for 1 h. Then, an aqueous suspension of ce-MoS_2 flakes (0.28 mmol) was added and stirred at room temperature for 24 h. After, the solid was filtered, washed with water, DMSO, and MeOH and dried under vacuum for 14 h in the darkness, at least.

MoS_2-3c. A solution of **1o** (12.30 mg, 0.028 mmol) in 40 mL of MeOH was subjected to UV irradiation (350 nm) in a photoreactor during 15 min under vigorous magnetic stirring. The resulting dark purple solution was rotary evaporated to yield a purple solid (**1c**). Finally, the procedure described for the synthesis of **MoS_2-3o** was followed.

Physical mixture

ce-MoS_2+3-Ho. The physical mixture of ce-MoS_2 with **3-Ho** was prepared by grinding 7.2 mg of ce-MoS_2 flakes and 2.3 mg of **3-Ho** in a mortar (**3-Ho**/MoS_2 molar ratio of ≈0.1).

1.3 Characterisation

Nuclear magnetic resonance spectroscopy (RMN). ^{1}H-RMN data were recorded at room temperature on a Bruker DPX300 spectrophotometer. Chemical shifts are reported in ppm, and they are referenced to $CDCl_3$.

Electrospray mass spectroscopy (ESI-MS). High-resolution ESI-MS in methanol solution were obtained on an AB SCIEX TripleTOF™ 5600 LC/MS/MS System.

Liquid UV/Vis spectroscopy. Spectra were recorded using Hellma quartz cuvettes and on a Jasco V-670 spectrophotometer and powder UV/Vis spectra were recorded using the PIN-757 adaptor.

Infrared spectroscopy. Spectra (4000–400 cm^{-1}) were recorded on a Nicolet 5700 spectrophotometer as KBr pellets. All samples were measured as KBr pellets, and transmittance intensities were scaled for comparison purposes.

Raman spectroscopy. Spectra were recorded with a Horiba-LabRam HR Evolution Spectrometer in ambient conditions. The measurements were performed with 8 mW (532 nm), 17 mW (633 nm) and 26 mW (785 nm) excitation power. A spot size of ~2μm diameter was used for all experiments. The spectrophotometer is equipped with laser filters that allow to diminish the laser beam power by selecting 0.1, 0.5, 1, 5, 10, 25, 50 100% laser power.

X-ray powder diffraction (XRPD). XRPD patterns were performed on a Panalytical Empyrean X-ray diffractometer by using Cu Kα radiation (λ= 1.5406 Å), in which the X-ray tube was operated at 45 kV and 40 mA ranging from 2 to 90°. The XRPD data was background corrected with the HighScore Plus software.

Thermogravimetric analysis (TGA). Experiments were conducted using a TA Instrument TGA550 in the 25–700 °C range under a 10 °C min^{-1} scan rate and N_2 flow of 100 mL min^{-1}.

X-ray photoelectron spectroscopy (XPS). XPS spectra were analysed using a Thermo Scientific K-alpha X-ray photoelectron spectrometer, using a monochromatic Al Kα radiation (1486.6 eV) at a pressure of $4 \cdot 10^{-9}$ mBar. XPS data were analysed with Avantage software, where the binding energy of the C 1s at 284.8 eV was used as reference to adjust the position of the other peaks.

1.4 Photoswitching studies

Photoreactor experiments. 1–**3-H** diarylethene molecules were irradiated inside a commercial photoreactor (LuzChem LZC-4V), with 14 UVB (308 nm) lamps, 14 UVA FL8BL-B (350 nm) lamps and 12 Sylvania Cool White F8T5 (visible) lamps with LuzChem orange filters (>540 nm).

Raman experiments. MoS_2-2 and **MoS_2-3** were deposited onto clean SiO_2 (285 nm)/Si substrates by drop-casting of their suspensions. Raman spectra were collected at 532 nm with 1% laser power. To induce photoswitching reactions, samples were irradiated with Raman lasers at different wavelengths (532 and 633 nm) with 5% laser power at different times. Next, Raman spectra were recorded on the same spot area with the Raman spectrophotometer at 532 nm with 1% laser power. Irradiating the samples with lower laser powers led to very noisy measurements, and at higher powers resulted in MoS_2 oxidation and sample burnings.

2 Ce-MoS_2 characterisation

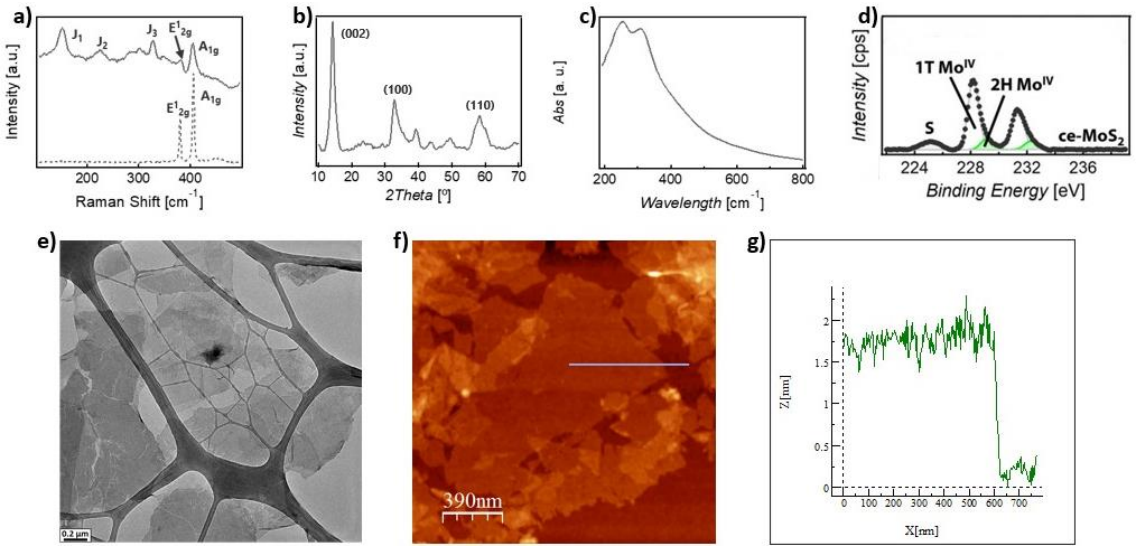

Fig. S1 Raman spectra of ce-MoS_2 (top) and commercial 2H-MoS_2 (down) measured at 532 nm excitation wavelength, b) PXRD pattern of ce-MoS_2, c) UV/Vis absorption spectrum of ce-MoS_2 in water d) XPS spectrum of ce-MoS_2, e) TEM image of ce-MoS_2 flakes, f) AFM topographic image of ce-MoS_2 flakes, g) Height profile of a ce-MoS_2 flake shown in f).

3 TEM characterisation

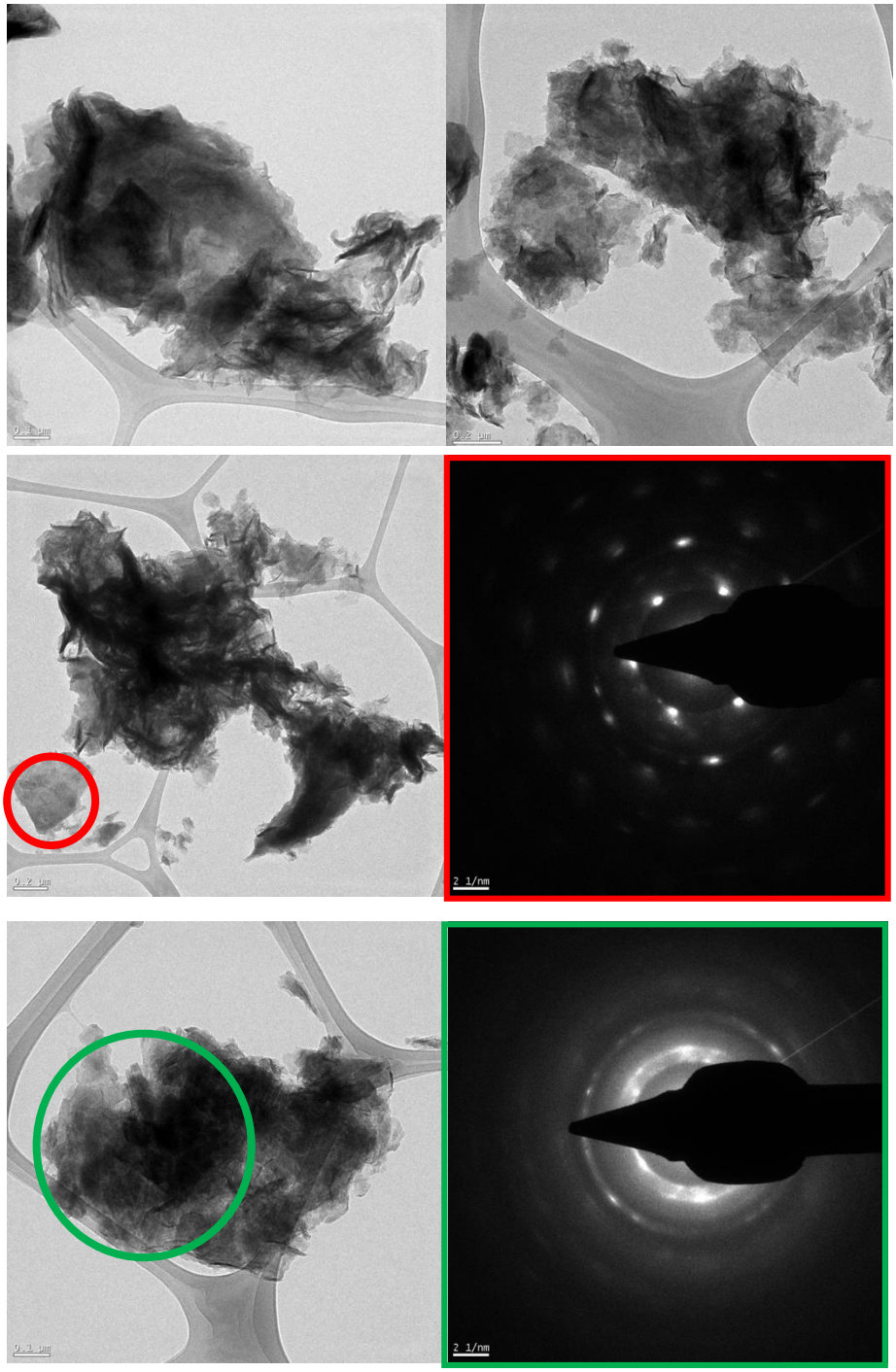

Fig. S2. Top: TEM images of **MoS_2-3o** (left) and **MoS_2-3c** (right). Middle: TEM image (left) of **MoS_2-3o** and SAED image (right) of a non-wrinkled region circled in red. Bottom: TEM image (left) of **MoS_2-3c** and SAED image (right) of a wrinkled region circled in green.

4 IR spectroscopy

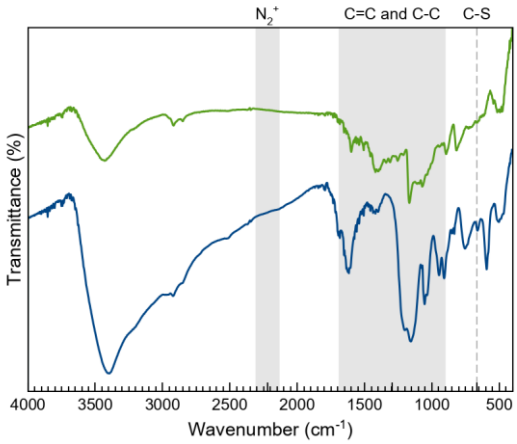

Fig. S3. FTIR spectra of **MoS_2-2c** (green) and **MoS_2-3c** (blue).

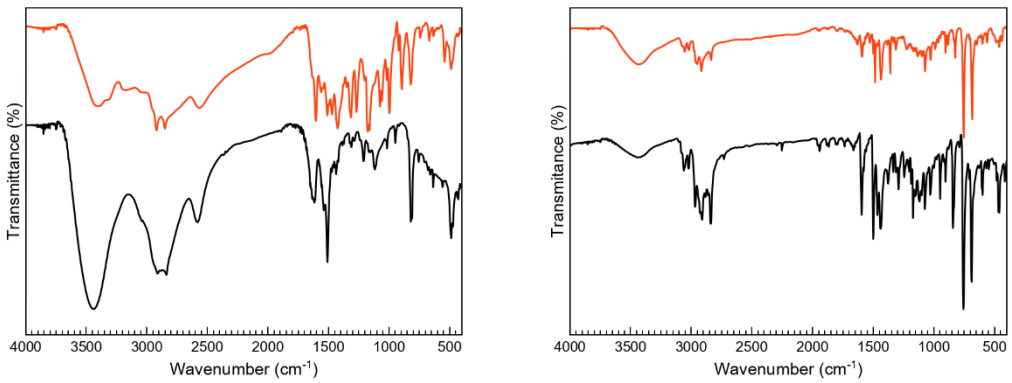

Fig. S4. FTIR spectra for the open (black) and closed (orange) forms of **2** (left) and **3-H** (right).

5 XPS spectroscopy

Table S1. XPS values observed in **1o**, **MoS_2-2** and **MoS_2-3**.

Mo peaks (eV)	S peaks (eV)	N peaks (eV)
1o		
	~163.7 S^{2-} $2p_{3/2}$ (S–C)	~399.4 N 1s (NH_2)
	~164.9 S^{2-} $2p_{1/2}$ (S–C)	
MoS_2-2o and MoS_2-2c		
~228.2 Mo^{IV} $3d_{5/2}$ (1T MoS_2)	~161.1 S^{2-} $2p_{3/2}$ (1T MoS_2)	~399.4 N 1s (NH_2)
~228.9 Mo^{IV} $3d_{5/2}$ (2H MoS_2)	~161.8 S^{2-} $2p_{3/2}$ (2H MoS_2)	
~229.9 Mo^{IV} $3d_{5/2}$ (MoO_2)	~162.2 S^{2-} $2p_{1/2}$ (1T MoS_2)	
~231.4 Mo^{IV} $3d_{3/2}$ (1T MoS_2)	~162.9 S^{2-} $2p_{1/2}$ (2H MoS_2)	
~232.1 Mo^{IV} $3d_{3/2}$ (2H MoS_2)	~163.7 S^{2-} $2p_{3/2}$ (S-C)	
~232.5 Mo^{VI} $3d_{5/2}$	~164.9 S^{2-} $2p_{1/2}$ (S-C)	
~233.0 Mo^{IV} $3d_{3/2}$ (MoO_2)	~226.1 S^{2-} 2s	
~235.7 Mo^{VI} $3d_{3/2}$		
MoS_2-3o and MoS_2-3c		
~228.8 Mo^{IV} $3d_{5/2}$ (2H MoS_2)	~161.2 S^{-} $2p_{3/2}$	
~229.9 Mo^{IV} $3d_{5/2}$ (2H MoO_2)	~161.8 S^{2-} $2p_{3/2}$ (2H MoS_2)	
~231.0 Mo^{V} $3d_{5/2}$	~162.1 S^{-} $2p_{1/2}$	
~232.0 Mo^{IV} $3d_{3/2}$ (2H MoS_2)	~162.9 S^{2-} $2p_{1/2}$ (2H MoS_2)	
~233.0 Mo^{IV} $3d_{3/2}$ (2H MoO_2)	~163.7 S^{2-} $2p_{3/2}$ (S–C)	
~234.3 Mo^{V} $3d_{3/2}$	~164.9 S^{2-} $2p_{1/2}$ (S–C)	
	~226.2 S^{2-} 2s	

5 Molecular representation of 3-H

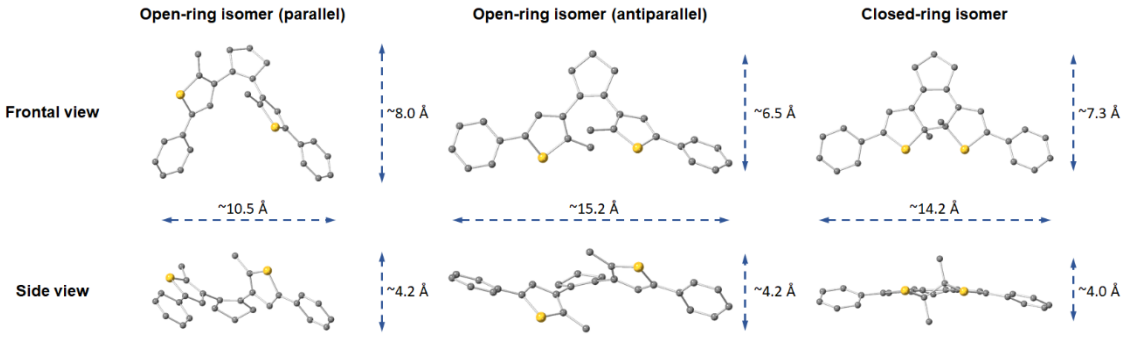

Fig. S5. Frontal- and side-views of the open isomer in the parallel (not suitable for photoswitching behavior) and antiparallel configurations, and the closed isomer of **3-H** in crystals.

6 Raman spectroscopy

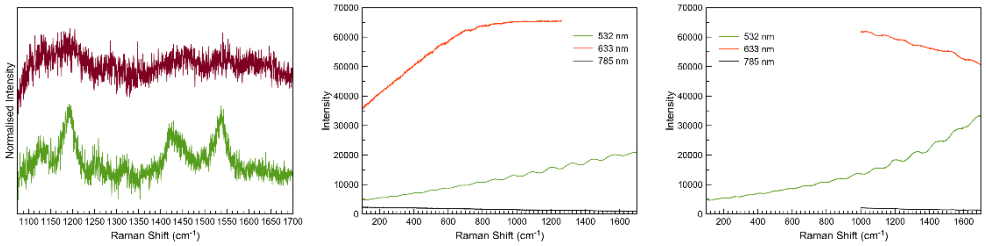

Fig. S6. Normalised Raman spectra of **2o** (red) and **2c** (green) as solid at 785 nm wavelength (left). Normalised Raman spectra of **2o** (middle) and **2c** (right) as solids at 532 (green), 633 (orange) and 785 nm (black) wavelengths**.**

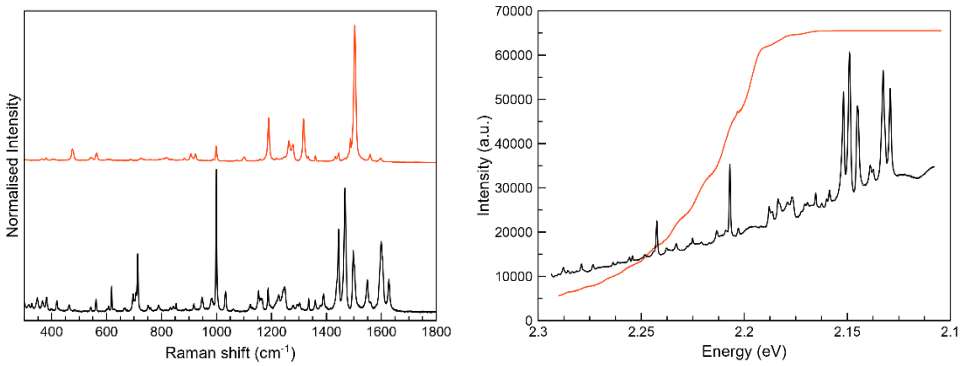

Fig. S7. Normalised Raman spectra of **3-Ho** (black) and **3-Hc** (orange) as solids at 785 nm wavelength (left). Photoluminescence spectra of **3-Ho** (black) and **3-Hc** (red) as solids at 532 nm (right).

7 TGA analysis

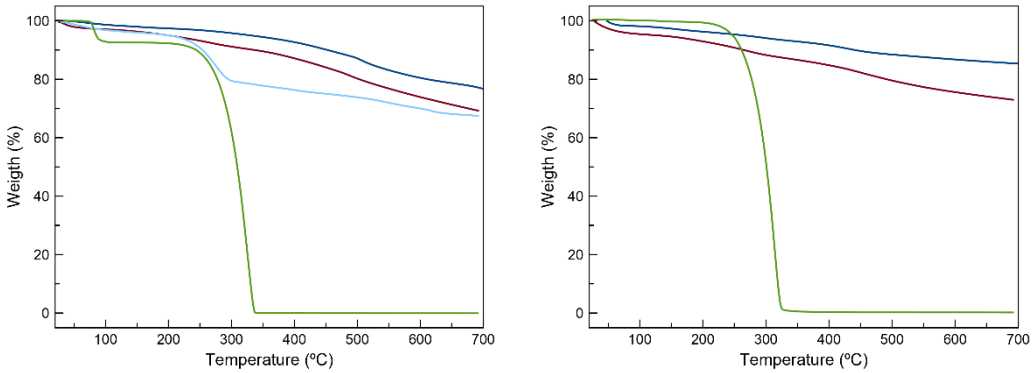

Fig. S8. TGA plots of **3-H** (green), physical mixture **ce-MoS_2+3-H** (light blue), **MoS_2-3** (red) and **MoS_2-2** (dark blue) for open (left) and closed (right) isomers.

8 Photoswitching behaviour

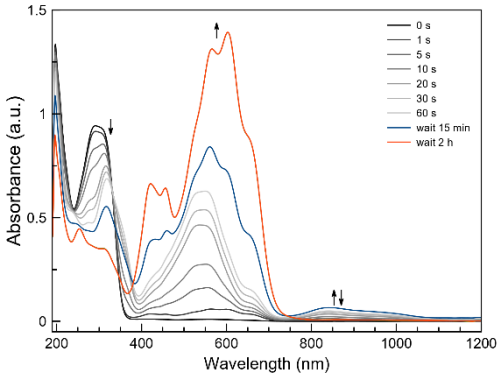

Fig. S9. UV/Vis absorption spectra of **2o** in EtOH/H_2O (70%) at different irradiation times with 350 nm lamps (grey gradient). Evolution of the spectra after protonation and irradiation at different times (blue and red lines).

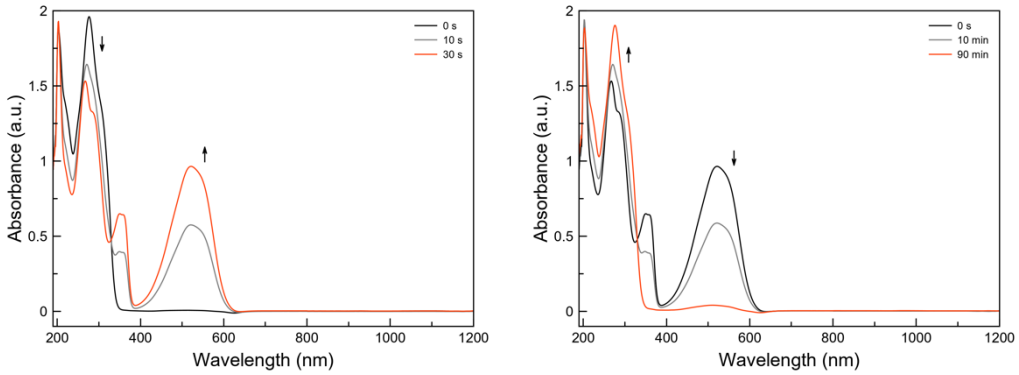

Fig. S10. UV/Vis absorption spectra of **3-H** in MeOH at different irradiation times with 308 nm (left) and visible lamps with >540 nm orange filters (right).

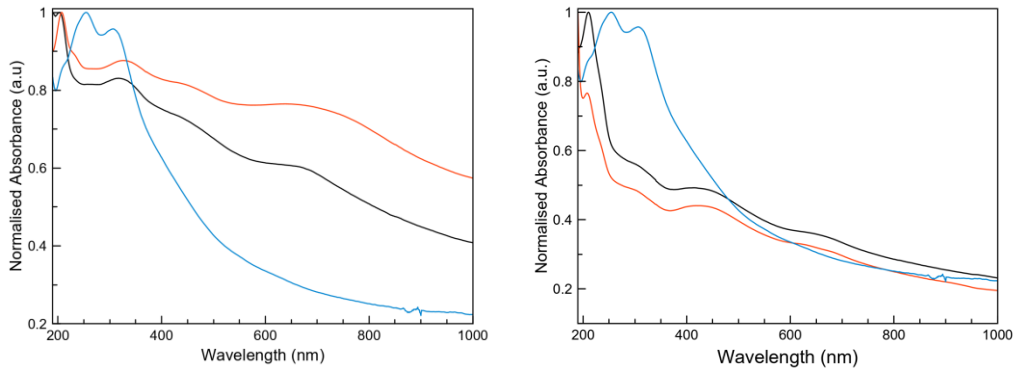

Fig. S11. UV/Vis absorption spectra of aqueous suspensions of **MoS_2-2** (left) and **MoS_2-3** (right) for the open (black) and closed (red) isomers and ce-MoS_2 (blue).

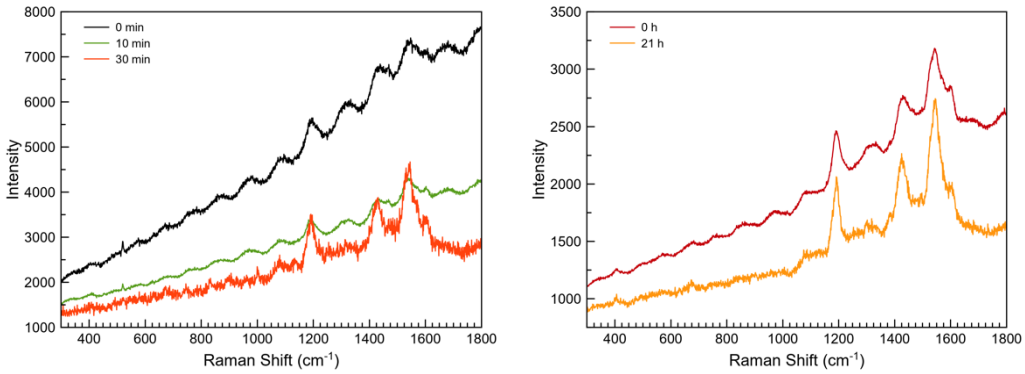

Fig. S12. Raman spectra of **2o** deposited onto a SiO_2/Si substrate by drop casting and measured at 532 nm excitation wavelength before (black) and after irradiation experiments in a photoreactor with 350 nm lamps (left). Raman spectra of **2c** deposited onto a SiO_2/Si substrate by drop casting and measured at 532 nm excitation wavelength before (red) and after (orange) irradiation experiments in a photoreactor with visible lamps with >540 nm orange filters (right).

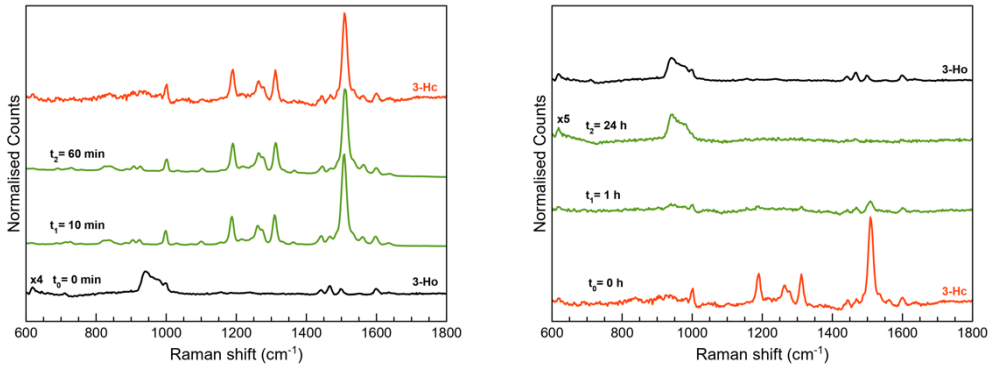

Fig. S13. Raman spectra of **3-Ho** (left) and **3-Hc** (right) deposited onto a SiO_2/Si substrate by drop casting and measured at 785 nm excitation wavelength before and after irradiation experiments in a photoreactor. The spectra were baseline corrected and some spectra were magnified for comparison purposes. A partial degradation upon the closed-ring aperture cannot be discarded because of the weak signals registered after the irradiation, even though the peak intensity of **3-H** is substantially low when drop-casted on the SiO_2 substrate.

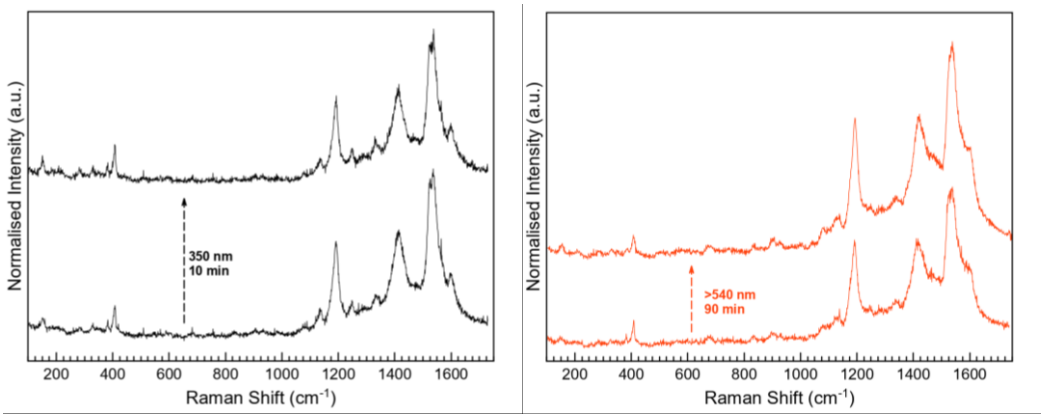

Fig. S14. Raman spectra at 532 nm of **MoS_2-2** deposited onto a SiO_2/Si substrate by drop casting and irradiated into a photoreactor at 350 nm (**MoS_2-2o**, left) and >540 nm (**MoS_2-2c**, right) for 90 minutes.

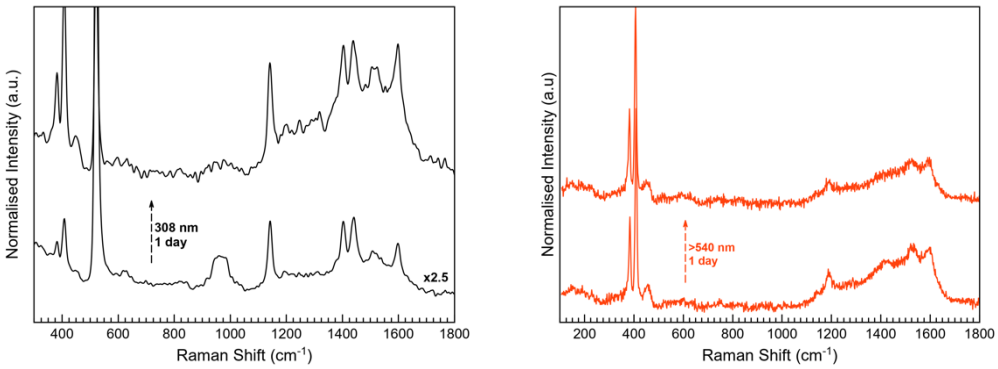

Fig. S15. Raman spectra at 532 nm of **MoS_2-3** deposited onto a SiO_2/Si substrate and irradiated into a photoreactor at 308 nm (**MoS_2-3o**, left) and >540 nm (**MoS_2-3c**, right) for 1 day.

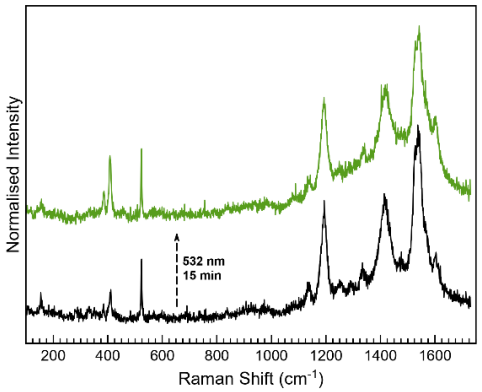

Fig. S16. Raman spectra at 532 nm for **MoS_2-2o** deposited onto SiO_2/Si substrates (black) by drop casting and the resulting irradiation using a 532 nm laser at 5% power (green).

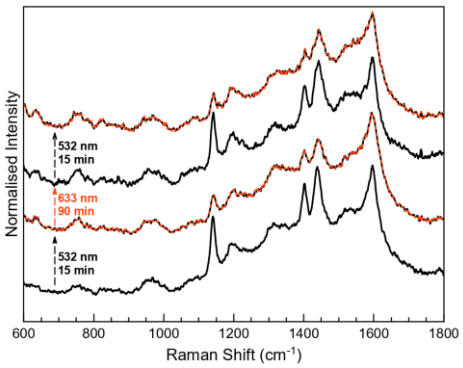

Fig. S17. Raman spectra for the irradiated **MoS_2-3o** sample deposited on SiO_2/Si by drop casting and measured with a 532 nm excitation laser with 1% laser power. The open- and the closed-ring isomers and the mixture of both of them are represented as black, red and black-red lines, respectively.

9. DFT and TDDFT calculations

Geometries of the open and closed form of **3-H** were optimised by PM6 semiempirical methods and DFT type calculations through the Gaussian 09 package by using the PBEPBE functional,[3-5] the quadratic convergence approach.[6,7] For the last method, a 6-31G all-electron basis set proposed by Pople *et al.* was used for all atoms.[8-17] The energies and oscillator strengths for less energetic electronic transitions were calculated on both optimised geometries obtained for the two different methods through the time-dependent formalism applied on the PBEPBE functional and using the 6-31G basis set.[18-24] Both procedures provide similar results and validate the geometry optimization through semiempirical methods when the computational cost is excessive for larger models. Thus, this optimization on a model of the photo-switchable molecule anchored to a MoS_2 surface (Fig. S18) is carried by this less expensive strategy. The estimation of the features of the excited states, or the energies and type of electronic excitations, is a crucial step in this study. In order to find relatively accurate results in a suitable time, the optimised geometry is frozen and simplified by reducing the layer to only the MoS_2 unity directly linked to the organic molecule. In this way, electronic effects are kept, but we should proceed with caution because they can be magnified (Fig. S18). However, for a semiquantitative analysis, this procedure can be successful enough. The TD-DFT calculations for this last model were done using a LanL2DZ electron-valence basis set and effective core potential for the molybdenum atoms.[25-28] Orbitals and spin densities maps were plotted through the Gabedit 2.5 software.[29]

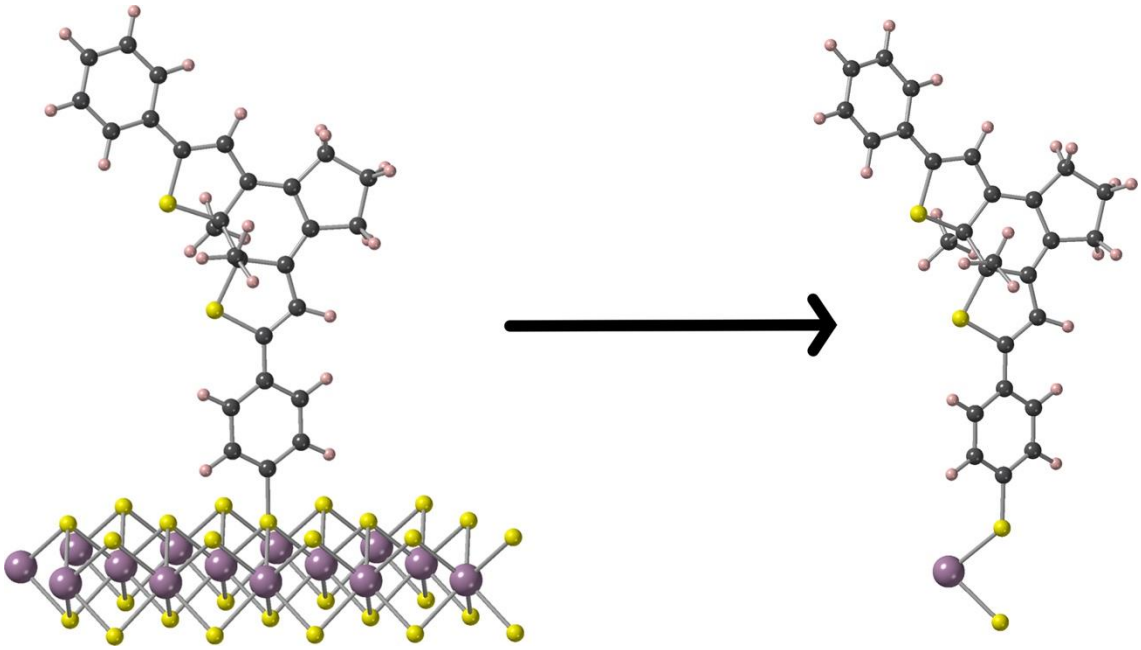

Fig. S18. Molecular model used to simulate **MoS_2-3o** and **MoS_2-3c** composites (left) and the subsequent simplification (right) applied to carry TD-DFT calculations.

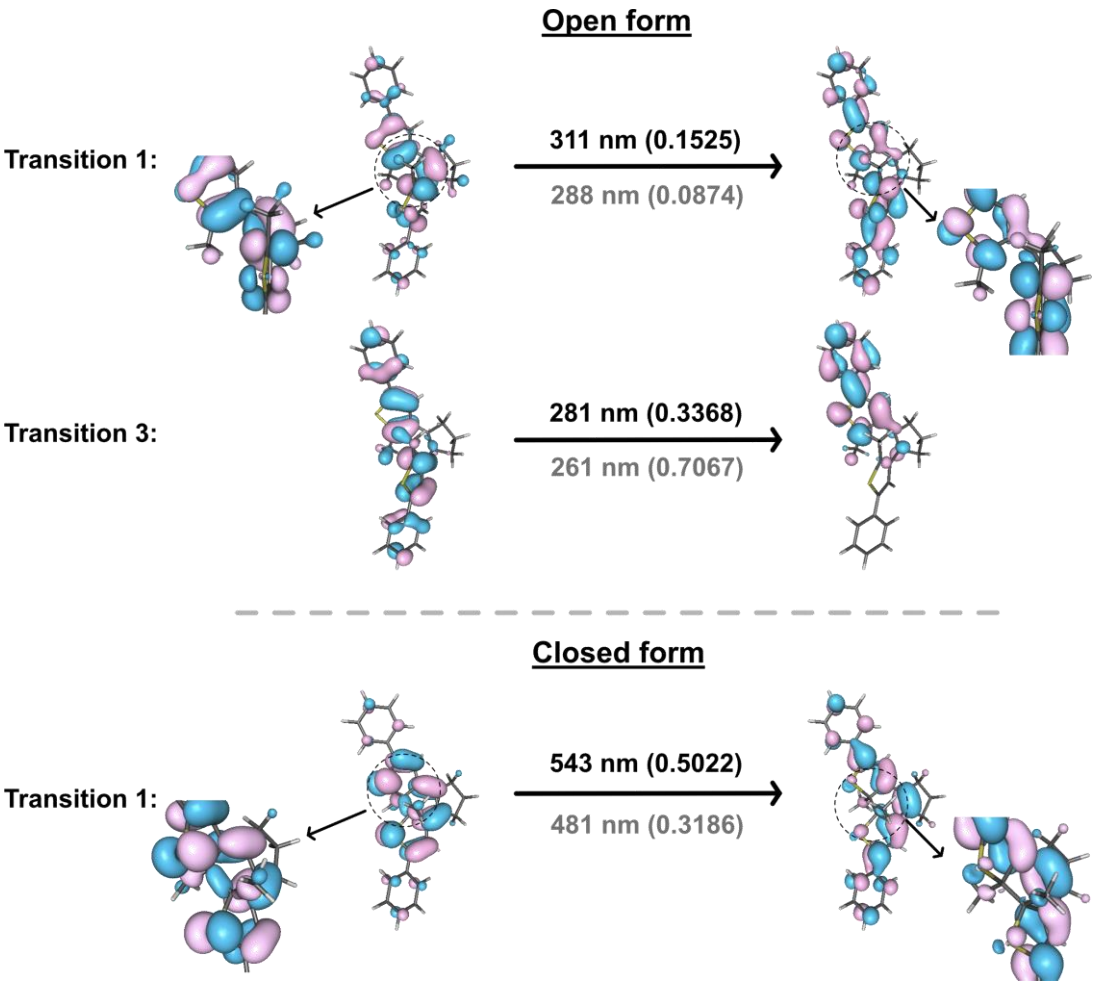

Fig. S19. Perspective views of the natural transition orbitals (NTOs) involved in some significant theoretical electronic excitations of the open and closed forms of the free organic molecule (**3-H**). The isodensity surfaces correspond to a cut-off value of 0.05 e bohr^{-3}. Electrons are promoted from the orbital at the left side to the other one at the right side. Oscillator strengths are given in parentheses. Results on DFT and PM6 optimised geometries appear in black and grey colours.

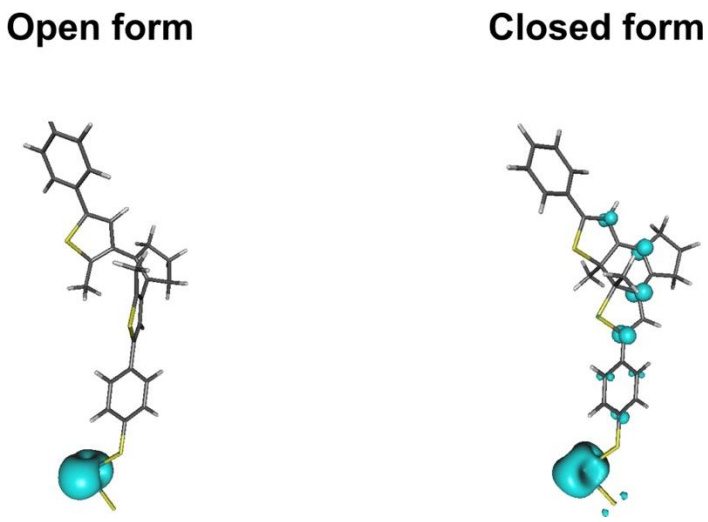

Fig. S20. Perspective views of the spin density distribution for the open and closed forms of the organic molecule anchored to the MoS_2. The isodensity surfaces correspond to a cut-off value of 0.005 e bohr^{-3}.

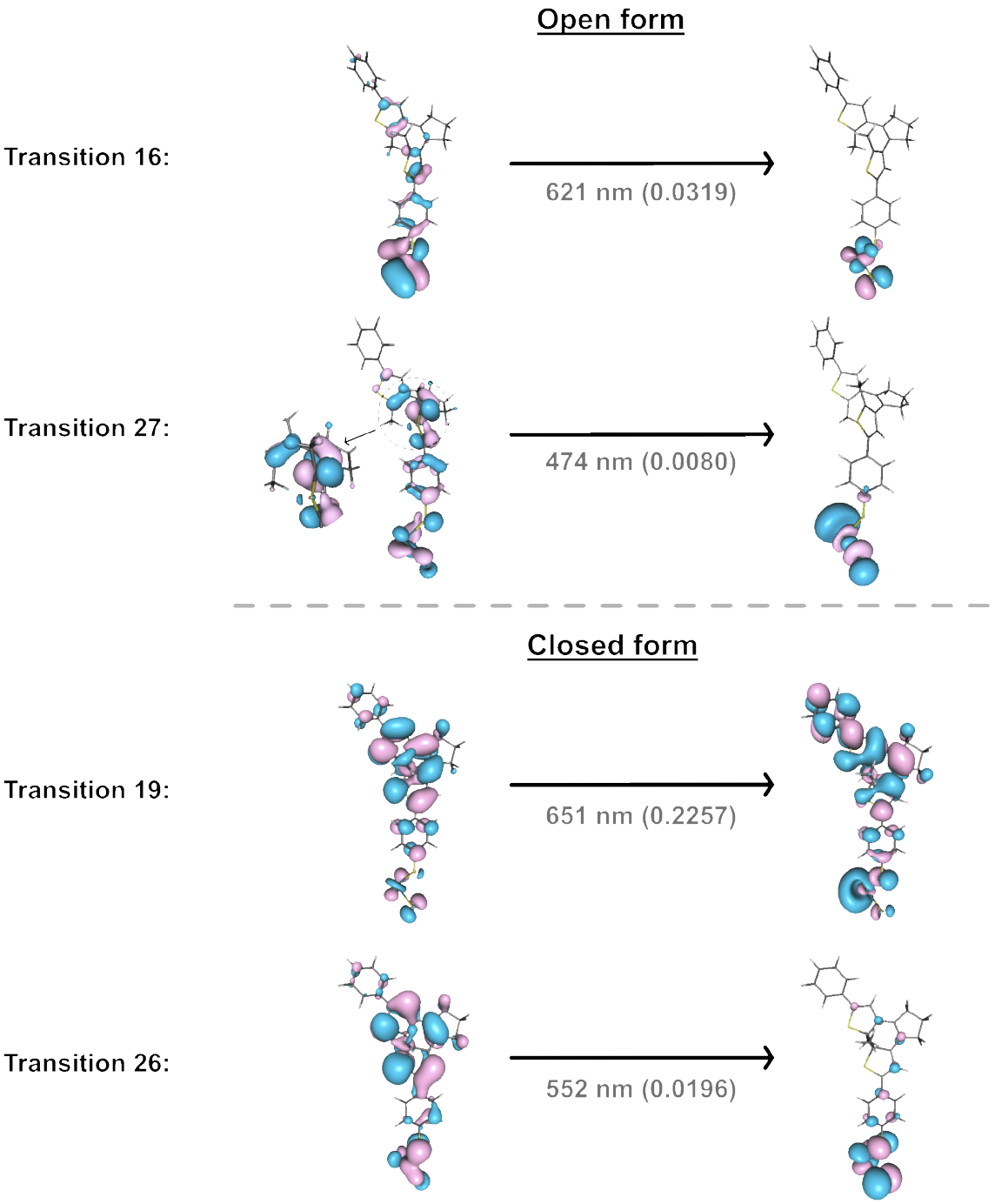

Fig. S21. Perspective views of the natural transition orbitals (NTOs) involved in some significant theoretical electronic excitations of the open and closed forms of the organic molecule anchored to a MoS_2 layer. The isodensity surfaces correspond to a cut-off value of 0.05 e bohr^{-3}. Electrons are promoted from the orbital at the left side to the other one at the right side. Oscillator strengths are given in parentheses. Results on PM6 optimised geometries appear in black and grey colours.

References

1 L. N. Lucas, J. J. D. De Jong, J. H. Van Esch, R. M. Kellogg and B. L. Feringa, *European J. Org. Chem.*, 2003, 155–166.

2 M. Morant-Giner, R. Sanchis-Gual, J. Romero, A. Alberola, L. García-Cruz, S. Agouram, M. Galbiati, N. M. Padial, J. C. Waerenborgh, C. Martí-Gastaldo, S. Tatay, A. Forment-Aliaga and E. Coronado, *Adv. Funct. Mater.*, 2018, **28**, 1706125.

3 J. J. P. Stewart, *J. Mol. Model.*, 2007, **13**,1173-213.

4 J. P. Perdew, K. Burke, and M. Ernzerhof, *Phys. Rev. Lett.*, 1996, **77**, 3865-3868.

5 J. P. Perdew, K. Burke, and M. Ernzerhof, *Phys. Rev. Lett.*, 1997, **78**, 1396.

6 G. B. Bacskay, *Chem. Phys.*, 1981, **61**, 385-404.

7 M. J. Frisch, G. W. Trucks, H. B. Schlegel, G. E. Scuseria, M. A. Robb, J. R. Cheeseman, G. Scalmani, V. Barone, B. Mennucci, G. A. Petersson, H. Nakatsuji, M. Caricato, X. Li, H. P. Hratchian, A. F. Izmaylov, J. Bloino, G. Zheng, J. L. Sonnenberg, M. Hada, M. Ehara, K. Toyota, R. Fukuda, J. Hasegawa, M. Ishida, T. Nakajima, Y. Honda, O. Kitao, H. Nakai, T. Vreven, J. A. Montgomery Jr., J. E. Peralta, F. Ogliaro, M. Bearpark, J. J. Heyd, E. Brothers, K. N. Kudin, V. N. Staroverov, R. Kobayashi, J. Normand, K. Raghavachari, A. Rendell, J. C. Burant, S. S. Iyengar, J. Tomasi, M. Cossi, N. Rega, J. M. Millam, M. Klene, J. E. Knox, J. B. Cross, V. Bakken, C. Adamo, J. Jaramillo, R. Gomperts, R. E. Stratmann, O. Yazyev, A. J. Austin, R. Cammi, C. Pomelli, J. W. Ochterski, R. L. Martin, K. Morokuma, V. G. Zakrzewski, G. A. Voth, P. Salvador, J. J. Dannenberg, S. Dapprich, A. D. Daniels, Ö. Farkas, J. B. Foresman, J. V Ortiz, J. Cioslowski, D. J. Fox, *Gaussian 09,* Gaussian, Inc., Wallingford CT, **2009**.

8 R. Ditchfield, W. J. Hehre, and J. A. Pople, *J. Chem. Phys.*, 1971, **54**, 724.

9 W. J. Hehre, R. Ditchfield, and J. A. Pople, *J. Chem. Phys.*, 1972, **56**, 2257.

10 P. C. Hariharan and J. A. Pople, "Influence of polarization functions on molecular-orbital hydrogenation energies," *Theor. Chem. Acc.*, 1973, **28**, 213-22.

11 P. C. Hariharan and J. A. Pople, *Mol. Phys.*,1974, **27** 209-214.

12 M. S. Gordon, *Chem. Phys. Lett.*, 1980, **76**, 163-168.

13 M. M. Francl, W. J. Pietro, W. J. Hehre, J. S. Binkley, D. J. DeFrees, J. A. Pople, and M. S. Gordon, *J. Chem. Phys.*, 1982, **77**, 3654-3665.

14 R. C. Binning Jr. and L. A. Curtiss, *J. Comp. Chem.*,1990, **11**, 1206-1216.

15 J.-P. Blaudeau, M. P. McGrath, L. A. Curtiss, and L. Radom, *J. Chem. Phys.*,1997, **107**, 5016-5021.

16 V. A. Rassolov, J. A. Pople, M. A. Ratner, and T. L. Windus, *J. Chem. Phys.*, 1998, **109**, 1223-1229.

17 V. A. Rassolov, M. A. Ratner, J. A. Pople, P. C. Redfern, and L. A. Curtiss, *J. Comp. Chem.*, 2001, **22**, 976-984.

18 R. Bauernschmitt and R. Ahlrichs, *Chem. Phys. Lett.*, 1996, **256**, 454-464.

19 M. E. Casida, C. Jamorski, K. C. Casida, and D. R. Salahub, *J. Chem. Phys.*, 1998, **108**, 4439-4349.

20 R. E. Stratmann, G. E. Scuseria, and M. J. Frisch, *J. Chem. Phys.*,1998, **109**, 8218-8124.

21 C. Van Caillie and R. D. Amos, *Chem. Phys. Lett.*, 1999, **308**, 249-255.

22 C. Van Caillie and R. D. Amos, *Chem. Phys. Lett.*, 2000, **317**, 159-164.

23 F. Furche and R. Ahlrichs, *J. Chem. Phys.*, 2002, **117**, 7433-7447.

24 G. Scalmani, M. J. Frisch, B. Mennucci, J. Tomasi, R. Cammi, and V. Barone, *J. Chem. Phys.*, 2006, **124**, 094107: 1-15.

25 T. H. Dunning Jr. and P. J. Hay, in *Modern Theoretical Chemistry*, Ed. H. F. Schaefer III, Vol. 3 (Plenum, New York, 1977) 1-28.

26 P. J. Hay and W. R. Wadt, *J. Chem. Phys.*, 1985, **82**, 270-283.

27 W. R. Wadt and P. J. Hay, *J. Chem. Phys.*, 1985, **82**, 284-298.

28 P. J. Hay and W. R. Wadt, *J. Chem. Phys.*, 1985, **82**, 299-310.

29 A.R. Allouche, *J. Comput. Chem*., 2011, **32**, 174-182.